

Multidirectional Pixelated Cubic Antenna with Enhanced Isolation for Vehicular Applications

Md. Amanath Ullah, *Graduate Student Member, IEEE*, Rasool Keshavarz, *Member, IEEE*, Justin Lipman, *Senior Member, IEEE*, Mehran Abolhasan, *Senior Member, IEEE* and Negin Shariati, *Member, IEEE*

Abstract—This paper presents a pixelated cubic antenna design with enhanced isolation and diverse radiation pattern for vehicular applications. The design consists of four radiating patches to take advantage of a nearly omnidirectional radiation pattern with enhanced isolation and high gain. The antenna system with four patches has been pixelated and optimized simultaneously to achieve desired performance and high isolation at 5.4 GHz band. The antenna achieved measured isolation of more than -34 dB between antenna elements. The overall isolation improvement obtained by the antenna is about 18 dB compared to a configuration using standard patch antennas. Moreover, isolation improvement is achieved through patch pixelization without additional resonators or elements. The antenna achieved up to 6.9 dB realized gain in each direction. Additionally, the cubic antenna system is equipped with an E-shaped GPS antenna to facilitate connectivity with GPS satellite. Finally, the antenna performance has been investigated using a simulation model of the vehicle roof and roof rack. The reflection coefficient, isolation and radiation patterns of the antenna remains unaffected. The antenna prototype has been fabricated on Rogers substrate and measured to verify the simulation results. The measured results correlate well with the simulation results. The proposed antenna features low-profile, simple design for ease of manufacture, good radiation characteristics with multidirectional property and high isolation, which are well-suited to vehicular applications in different environments.

Index Terms—Connectivity, high-gain antenna, high isolation, multidirectional, pixelated antenna, PSO algorithm, vehicular communications.

I. INTRODUCTION

THE use of wireless technology is ubiquitous in our everyday lives. After a few decades of focusing on the development of wireless systems, there is now increased attention to vehicular communications [1-3]. Communication between vehicles can be incorporated into a telemetric platform to supply the driver with real-time information. To provide a better user experience, mobile and wireless connectivity in vehicles is gaining increasing interest from academia and industry. A wireless local area network (WLAN) system for internet access from any location, as well as vehicle-to-vehicle communication systems for safe driving

This Manuscript submitted on June 17, 2023.

In undertaking this work, we would like to acknowledge the partial support of Food Agility Cooperative Research Centre (CRC) Ltd, funded under Commonwealth Government CRC Program. One of us (M.A.U.) would also like to acknowledge the receipt of a Top-up Postgraduate Scholarship from Food Agility CRC. The CRC Program supports industry-led collaboration between industry, research and the community.

control could be included in future vehicles. Radio frequency (RF) systems such as Satellite Digital Audio Radio Service (SDARS), Global Positioning System (GPS), Vehicle to-Everything (V2X) communication, cellular communication, and Wireless Local Area Network (WLAN) are increasingly installed in modern automobiles for navigation, communication, and entertainment purposes [1, 4-7].

A vehicle's antenna design is challenged by stringent requirements. Vehicular communication modules require low-profile antennas with multi-standard characteristics, such as good radiation performance with the ability to communicate in multiple directions, enhanced isolation from antenna elements, high gain and high bandwidth. Increased coverage, enhanced robustness to multipath, and resistance to signal interception and interference are some of the benefits that smart antennas offer over standard antennas. Also, smart antennas have the ability to determine the direction of arrival (DOA) of an incoming signal and adjust the radiation pattern to enhance smart vehicular localization systems [8, 9].

A multidirectional antenna system is a promising approach to meet the requirements of vehicular technologies. There is a greater chance of improved signal reception if the antenna has more radiators. Because of this feature, the antenna can establish a reliable connection even when the vehicle is in motion. Simple omnidirectional patch antennas can be utilized for this purpose as omnidirectional antennas may receive signals from any direction (both in terms of elevation and azimuth), but their gain is typically quite low [10]. In such a scenario, the receiver may feature a number of antennas oriented in various directions to detect signals in its various polarizations. The quality of the received signal is enhanced by employing appropriate switching/selection or combining strategies.

In such a scenario, the issue of mutual coupling comes into effect when multiple antenna elements are closely placed together. Antennas should be as far apart as possible from one another to minimize interference from nearby radiators and maintain signal quality.

Authors are with RF and Communication Technologies (RFCT) research laboratory, Faculty of Engineering and IT, University of Technology Sydney, Ultimo, NSW 2007, Australia.

M. A. Ullah and Negin Shariati. are also with Food Agility CRC Ltd, 175 Pitt St, Sydney, NSW 2000, Australia.
E-mail: mdamanath.ullah@student.uts.edu.au

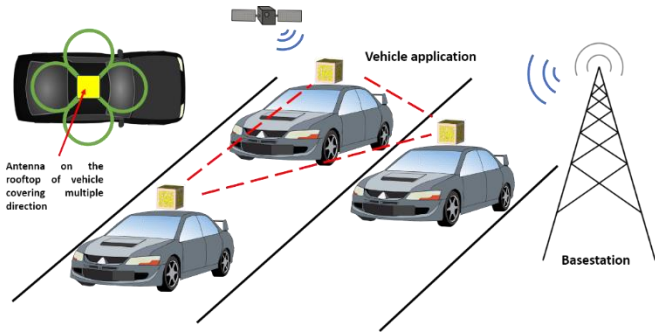


Fig. 1. Potential vehicular application scenario of the proposed multidirectional antenna in outdoor environment.

Therefore, the best way to establish a solid connection is through increased isolation [6, 11, 12]. Different attempts have been made by the antenna research community to improve isolation. The defected ground structure (DGS) is a common technique for reducing mutual coupling [13-15]. Nevertheless, antenna radiation performance is impacted when the DGS is used as a decoupling element. As a result, improved isolation comes at the expense of radiation performance. Considerable separation between the antenna elements is required to reduce mutual coupling using the split-ring resonators (SRR) [16] and electromagnetic bandgap (EBG) [17] structures [18]. In addition, other mutual coupling reduction techniques include slotted meander-line resonators (SMLR) [19], metamaterial structures [20] and parasitic elements [21] between antennas. However, such methods involve utilization of extra space within the antenna structure, as they are mostly used as separate elements or resonators to suppress mutual coupling. In addition to increasing the antenna size, they may affect the antenna performance.

As seen in Fig. 1, multidirectional antenna systems can facilitate real-time, traffic-based adjustment of the coverage area. High-efficiency and energy-saving communication is therefore possible. Vehicle antennas should be able to communicate in multiple directions to provide communication dependability between the vehicle and other wireless infrastructure, particularly in the case of long-distance, wide-area coverage, and high-speed data transmission.

In this paper, we propose a multidirectional cubic shaped antenna system with enhanced isolation and high gain. The structure consists of four antennas with pixelated configurations on the patches. The antenna design is based on binary optimization of the radiating patches while focusing on two design goals of reflection coefficient at the desired frequency (5.4 GHz) and isolation improvement. This work suggests combining polarization diversity measures to simultaneously take advantage of omnidirectional patterns with high gain. To increase the possibility of capturing wireless signals, multiple directional antennas are arranged in the cubic structure configuration. The antenna is designed using a binary optimization algorithm with pixelization of the radiating patches.

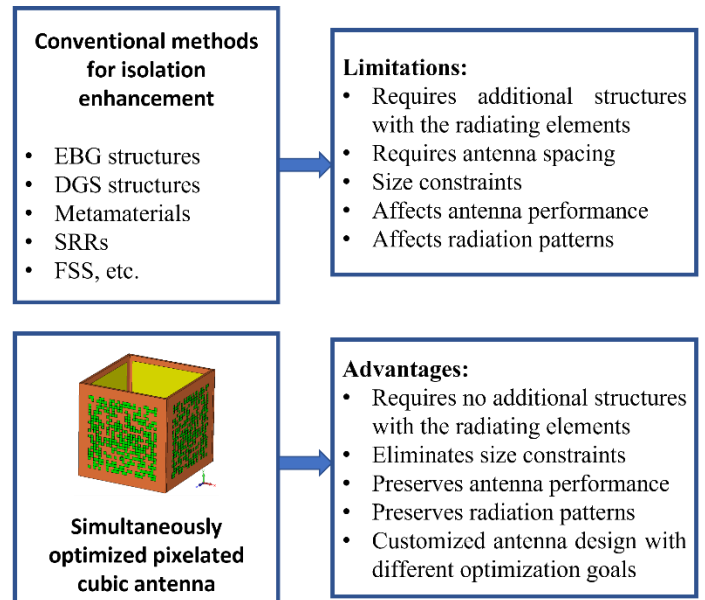


Fig. 2 Overview of the proposed antenna method: advantages over traditional design techniques to enhance isolation.

Exploration of different pixel configuration yielded desired results in previous dual-band antenna designs in [22, 23], where different kind of pixelated patch has been used to achieve operation in different frequency. To the best of authors' knowledge, the pixel optimization implemented to enhance isolation of multi antenna system in this work without using additional resonators has not been implemented in any prior work. No extra resonator or parasitic element is placed between the antennas, facilitating a compact antenna profile, while maintaining desired performance with increased isolation. Moreover, an edge-to-edge gap between the radiating elements is not required in this design. Fig. 2 illustrates the proposed antenna design advantages over conventional methods to enhance isolation. The proposed antenna achieved up to 6.9 dBi realized gain. The measured results demonstrate that the isolation between the antennas is better than -34 dB. The overall improvement of 18 dB isolation is achieved in comparison to a standard patch antenna system. Additionally, an E-shaped patch has been placed on top of the cubic structure, which operates at GPS frequency of 1.57 GHz.

II. ANTENNA DESIGN CONFIGURATION AND OPTIMIZATION

This section outlines the design and optimization of the proposed cubic antenna. The antenna design initially starts with a standard patch antenna technique using simple rectangular radiating patches. The basic microstrip patch antenna is used to design and analyze the first configuration, in which the maximum lobe of the pattern is perpendicular to the patch. To take advantage of the cubic shape from a geometric point of view, the four microstrip patch antennas were placed in opposite and perpendicular directions. Each antenna is designed to operate at 5.4 GHz on Rogers 4003 substrate. The configuration is depicted in Fig. 3. In this configuration, each antenna has about 5 dBi realized gain with only 60 degree beamwidth. However, using standard patch antenna design is

not suitable for this configuration, as the mutual coupling between antennas is high, as depicted in Fig. 3. The maximum isolation between antennas achieved in this configuration is only about -18 dB (S21). Also, the simulated efficiency is around 55% in cubic configuration. Nevertheless, the efficiency of each antenna is 66.3% with 6.6 dBi of realized gain, when each patch antenna is simulated separately. A key challenge in multi-antenna system is the reduction of mutual coupling between antennas that affects each antenna element's radiation performance. Fig. 3(b) shows a mutual coupling of about -13 to -18 dB between the antennas. This configuration has degraded efficiency and radiation performance.

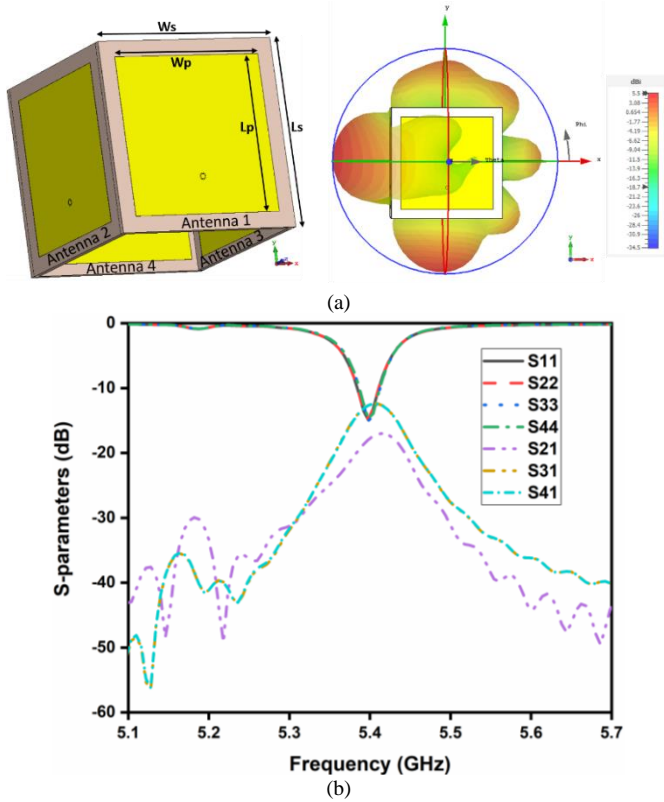


Fig. 3 Configuration of four simple patch antennas in a cubic structure and the simulation results; $W_s = L_s = 50$ mm, $W_p = L_p = 41.6$ mm.

To address these challenges, in the proposed antenna design, pixelization technique is used to reduce the mutual coupling effect while maximizing performance of each antenna in the cubic configuration. In this design, pixelization of the four patch antennas is performed simultaneously to achieve operating frequency at the desired band with high isolation. Unlike any previously reported methods, our design approach is based on patch shape optimization without placing any decoupling resonator. This also results in shrinking the antenna profile because only the defined area of the patch is considered.

Fig. 4(a) depicts the initial configuration of the proposed antenna. The antenna is designed on Rogers 4003 substrate with dielectric constant of 3.55 and 1.52 mm thickness. Each antenna of the cubic structure is fed by the co-axial feeding technique. The patch as a radiating element is subdivided into

26 \times 26 array of total 676 pixels. The array of pixels occupies 39mm \times 39mm, smaller than the standard patch size simulated in Fig. 3. Each pixel size is 1.5mm \times 1.5mm. Then each pixel is given a value of 0 or 1, denoting the elimination and presence of the copper layer in each pixel's defined area, respectively. Table 1 depicts the initial design dimensions of the antenna. Mirror technique has been employed to avoid using a large number of pixels, as shown in Fig. 4(b); the same pixel configuration is applied in all antennas during simulation. All antennas are considered simultaneously for the optimization process. Additionally, patches of antenna 1 and antenna 2 are arranged differently from antenna 3 and antenna 4 to achieve better isolation. The pixel configuration of antennas 3 and 4 is the reverse (side-by-side) of antennas 1 and 2. The feed point of the patch remains as a conductor during the optimization process to ensure excitation to the patch at all times.

TABLE I
DESIGN DIMENSIONS OF THE PROPOSED ANTENNA

Parameters	Value (mm)	Parameters	Value (mm)
W_{sp}	50	L_{sp}	50
W_{pp}	39	L_g	44
L_{pp}	39	W_g	44

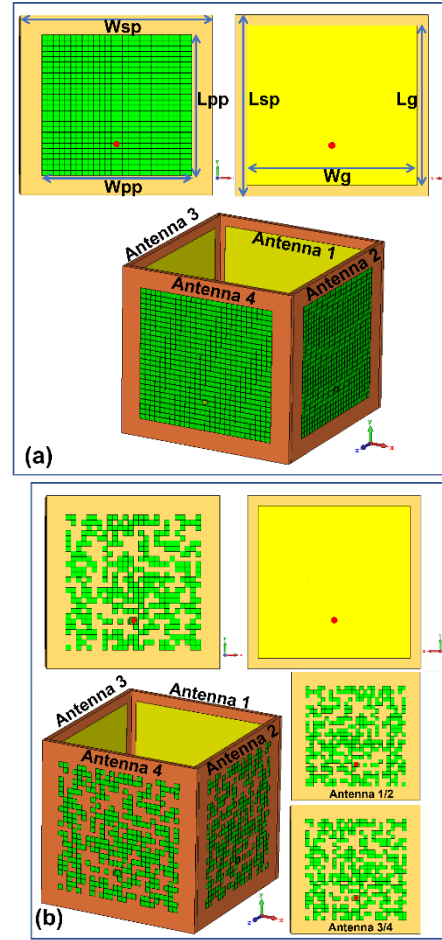


Fig. 4 Design Configuration and evolution of the proposed antenna (a) pixelization of the structure, (b) optimized pixelated configuration of the antenna.

The underlying mechanism of the optimization process is based on the inherent relationship between the pixel configuration and S-parameters of the antenna. Each generated pixel configuration introduces mini slots on the antenna patch. Modifications made to the radiation patch's slots can have a prominent impact on the antenna's performance, primarily caused by changes in the path of surface currents. The pixelization process of the patches is performed using a binary particle swarm optimization (PSO) algorithm with V-shaped transfer function (VBPSO) [24]. The configuration of pixel positions is optimized by the VBPSO. The following equations alter the particle's position and velocity in accordance with its prior position and velocity.

$$v_i^{t+1} = wv_i^t + c_1 \times rand \times (pbest_i - x_i^t) + c_2 \times rand \times (gbest - x_i^t) \quad (1)$$

$$x_i^{t+1} = x_i^t + v_i^{t+1} \quad (2)$$

Where, the velocity and position of particle i at iteration t is defined by v_i^t and x_i^t respectively. c_1 and c_2 denote the acceleration coefficient, and w represents a weighting function. A random number between 0 and 1 is shown by $rand$. Referring to equations (1) and (2), it becomes evident that the PSO algorithm is tailored for managing search spaces of a continuous nature. However, when confronted with discrete binary search spaces, novel optimization complexities emerge. Consequently, the resolution of these challenges necessitates the application of a binary algorithm, a prerequisite in addressing the optimization demands of the automated pixelated antenna design methodology. Notably, the discrete and continuous variants of the PSO exhibit contrasting features, encompassing a novel approach for updating positions and the introduction of an innovative transfer function aimed at converting a continuous search space into its binary counterpart. The following V-shaped transfer function in Equation (3) is adopted for the BPSO in the proposed antenna design to avoid local minima and premature convergence [24].

$$T(x) = |(x)/\sqrt{1+x^2}| \quad (3)$$

$$x_i^k(t+1) = \begin{cases} (x_i^k(t))^{-1} & \text{If } rand < T(v_i^k(t+1)) \\ x_i^k(t) & \text{If } rand \geq T(v_i^k(t+1)) \end{cases} \quad (4)$$

Utilizing Equation (3), real velocities were transformed into probabilities within the range of 0 to 1. Here, v_i^k represents the velocity of particle i along dimension k during iteration t . Once these velocities are converted into probabilities, Equation (4) can be employed to adjust the position vectors.

Table 2 illustrates the parameters used in the algorithm during optimization.

TABLE 2
PARAMETERS USED IN THE BPSO ALGORITHM

Number of iterations	60
c_1	1.5
c_2	2.5

Two design goals are considered in the proposed antenna design: achieving operation and enhancing isolation at 5.4 GHz frequency band. The frequency of operation is selected to prove the concept of the design process. Nevertheless, the frequency band can also be changed by altering the design goal in cost function. In order to achieve desired performance, the fitness function for the VBPSO optimizer is set by capturing the S parameters from EM simulator following several trials. We set the fitness function as a minimization problem. The reflection coefficient of antenna 1 (S11) is considered in Equation (5), where the transmission coefficients (S21, S31, S41) between all antennas are included. The reflection coefficients of all other antennas remain mostly similar due to the same pixel configuration on the patch.

$$FF = w_1(S11_{f=5.4 \text{ GHz band}}) + w_2((S21 + S31 + S41)_{f=5.4 \text{ GHz band}}) \quad (5)$$

The co-simulation is performed using binary optimization algorithm implemented in Matlab along with CST Microwave Studio EM simulator simultaneously. The following are the individual steps that were taken in the simulation and optimization process:

Step 1: Initialize particle positions. Set the number of maximum iterations.

Step 2: Calculate each particle's fitness value in accordance with equation (5). A binary bit string with 676 bits is sent to the EM simulator to generate pixel configurations. After simulation, the values of S parameters are sent back to Matlab to calculate the fitness value.

Step 3: Analyze each particle's fitness value. Then, update the personal best and global best position of particles.

Step 4: Velocity value is calculated and updated according to Equation (1). The position of particles is updated in accordance with Equations (2) and (3).

Step 5: Check the number of iterations. If the current number of iterations is less than the maximum iterations, return to Step 2. If maximum iterations are completed, proceed to Step 6.

Step 6: Save global best score and best position. The best position of particles provides the optimum pixel configuration of the antenna.

It takes up to 41 hours to complete the optimization procedure. However, a significant amount of simulation time is taken by the EM simulator to generate pixel configurations and simulate the cubic antenna structure. A small time is required by Matlab for implementing the algorithm. The fitness function used in Equation (5) resulted in efficient antenna optimization. Fig. 5

depicts the convergence curve of the optimization. As can be seen, the VBPSO algorithm converged at iteration 43. The fitness value decreased to a minimum value of -13.014 when the maximum number of iterations is completed.

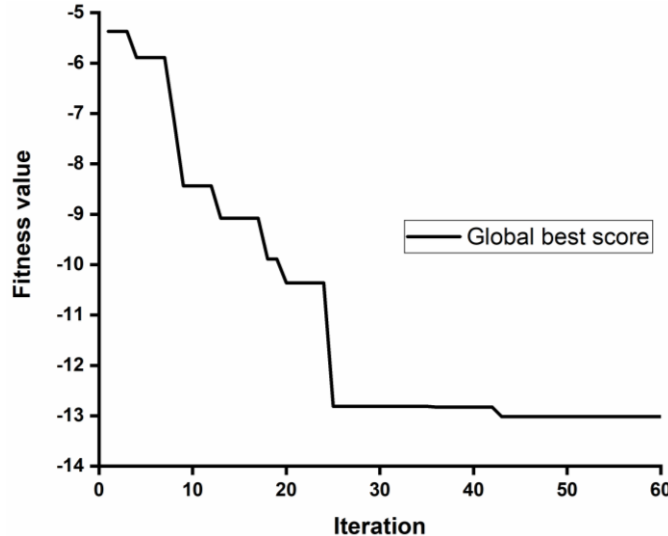
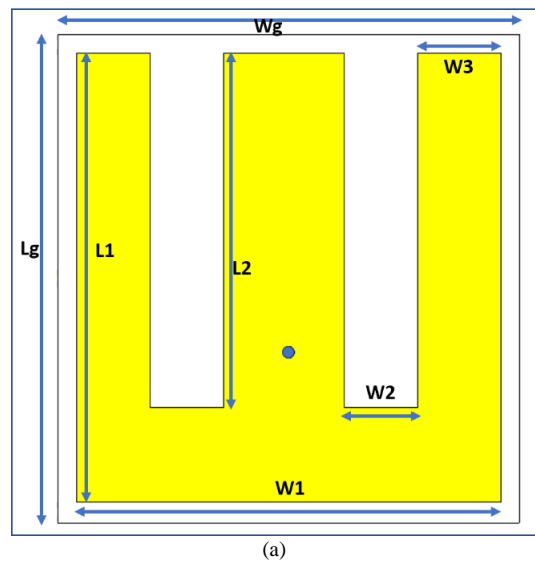


Fig 5. Convergence curve of the optimization.

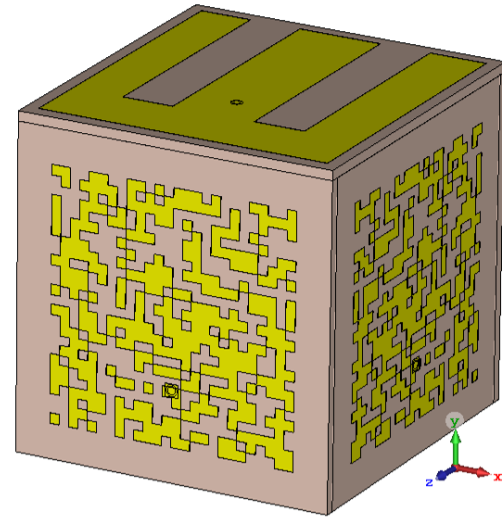
Additionally, a simple GPS patch antenna is placed on the topside of the cube shaped structure to facilitate the antenna system communication with GPS satellite. A simple E shaped radiating patch has been utilized to achieve an operating frequency of 1.57 GHz for the GPS antenna. The antenna is also designed on a Rogers 4003 substrate with 1.52 mm thickness. Fig. 6(a) depicts the design configuration of the E-shaped GPS antenna. Fig. 6(b) presents the position of GPS antenna on the topside of the pixelated optimized antenna. Table 3 provides the dimensions of GPS antenna.

TABLE 3. DIMENSIONS OF THE GPS ANTENNA

Parameters	Dimensions (mm)
L_g	48.75
W_g	46
L_1	48.75
L_2	38.5
W_1	46
W_2	8
W_3	9



(a)



(b)

Fig. 6 (a) E-shaped GPS antenna (b) placement of the antenna with cubic structure

III. SIMULATED AND MEASURED RESULTS

The antenna prototype is fabricated and tested to validate the performance of simulation model. The antenna with optimized pixel configurations has been fabricated on Rogers 4003 substrate and its performance has been measured. Photographs of the fabricated prototype and measurement setup are presented in Fig. 7. The simulated and measured results of the antennas' reflection coefficient are presented in Fig. 8. The simulated operating band is from 5.35 GHz to 5.47 GHz. The measured results illustrate that all four antennas resonate at a nearly similar frequency band to the simulation. They achieved -10 dB impedance bandwidth from 5.33-5.43 GHz. Good agreement between simulations and measurements is observed; nonetheless, a minor disparity is noted which may be attributable to fabrication imperfections.

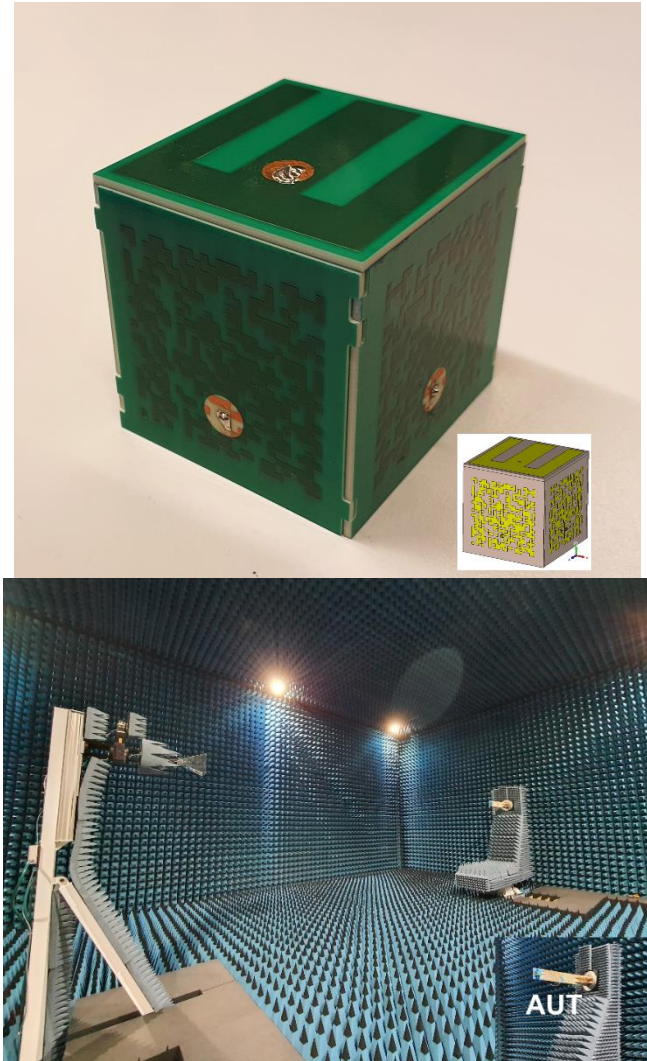


Fig. 7 (a) Fabricated prototype of the antenna (b) measurement setup of the antenna under test (AUT) in anechoic chamber

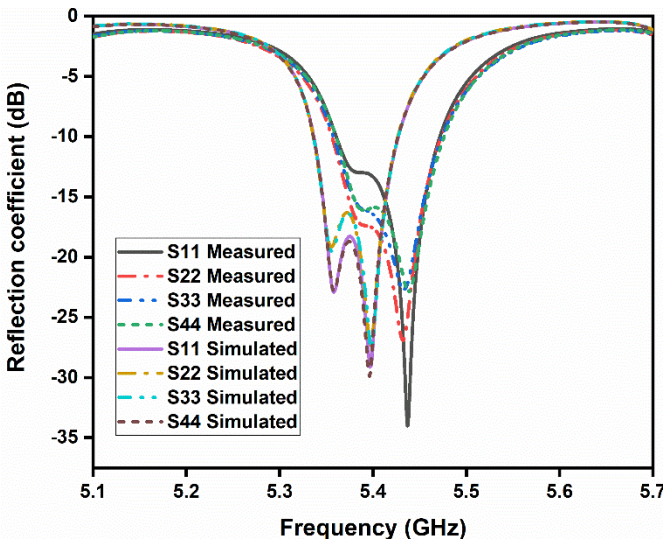


Fig. 8. Simulated and measured reflection coefficients of the antennas (Antenna 1, Antenna 2, Antenna 3 and Antenna 4)

Enhancing the isolation between antennas is the second design goal of the cubic antenna structure. Figure 9 represents the

simulated and measured S-parameters of the antennas. The antennas in the cubic structure are tightly packed, leading to large mutual coupling, as depicted in Fig 1. Hence, the isolation is enhanced using pixelated patch configuration without any decoupling resonator or components. The isolation value is below -34 dB at 5.4 GHz in simulation, and below -37 dB in measurement results. The maximum achieved isolation is -45 (S31 at 5.4 GHz) dB in simulation, while in measurement the maximum value is -42.5 dB (S31 at 5.43 GHz).

Surface current distribution is plotted in Fig. 10 to demonstrate the influence of pixelated patch configuration on the antenna elements in the cubic shaped structure. In Fig. 10 (a), when the antenna 4 is excited, the surface current is coupled from one antenna to another. However, the surface current is suppressed after the patch layout is optimized using pixelated configuration. The induced surface current in the nearby antenna has been significantly reduced and as a result, the isolation between antennas has increased.

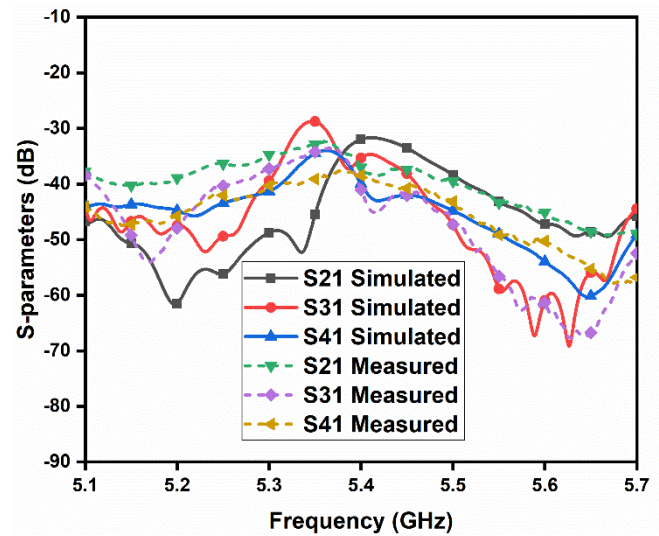


Fig. 9 Simulated and measured S-parameters of the antennas.

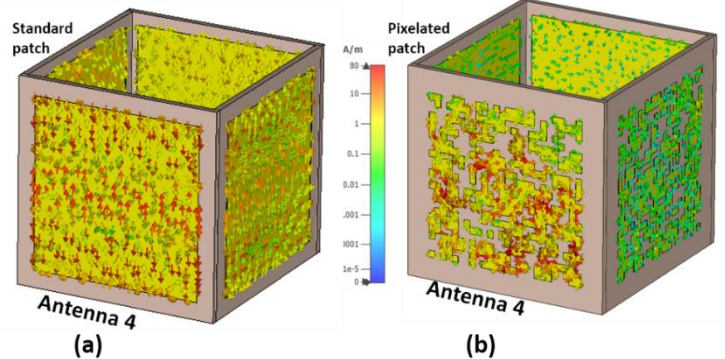


Fig. 10. Simulated surface current distribution, (a) with standard patch at 5.4 GHz (b) using optimized pixelated patch at 5.4 GHz

Fig. 11 presents the simulated and measured reflection coefficient of the GPS antenna. The antenna has been simulated and measured considering the placement on top of the four pixelated antennas structure. The measured results correlate well with the simulated results.

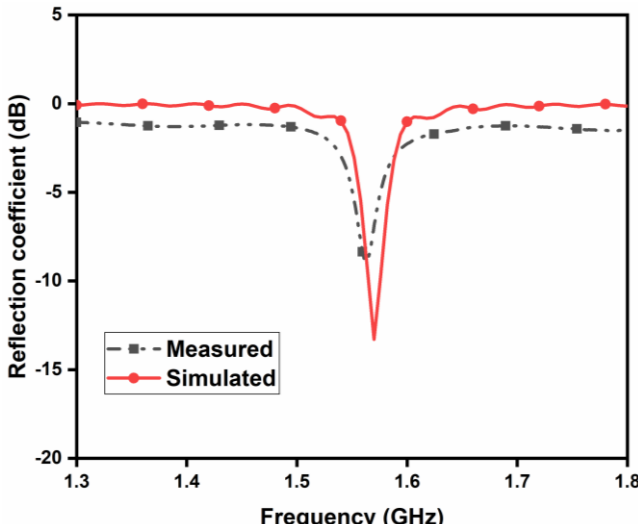
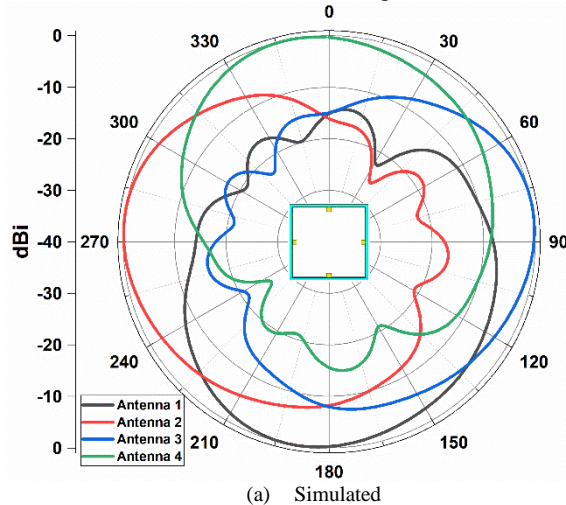
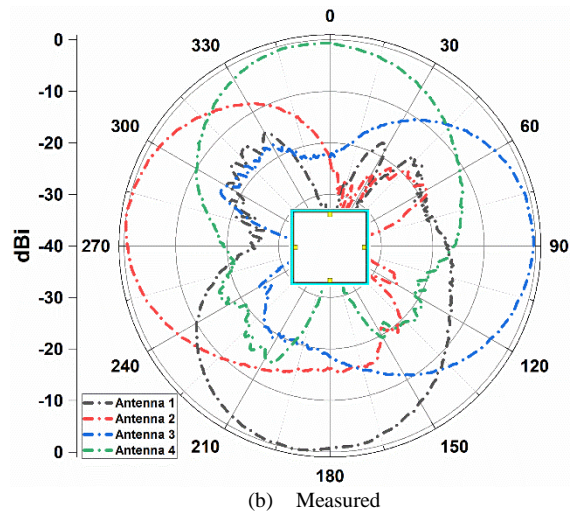


Fig. 11 Simulated and measured reflection coefficient of the GPS antenna

The simulated and measured H-plane and E-plane radiation patterns of the pixelated cubic antenna are shown in Fig. 12 and Fig. 13 respectively. The radiation patterns measurement is performed in the anechoic chamber shown in Fig. 7. The measured results of radiation patterns coincide well with the simulated results. The combined radiation pattern of four antennas covers all propagation directions in both planes. Moreover, it should be noted that, due to isolation enhancement using pixelated patch technique, the radiation patterns are not affected. The achieved maximum measured gain is 6.4 dBi, which is close to the simulated realized gain of 6.9 dBi.

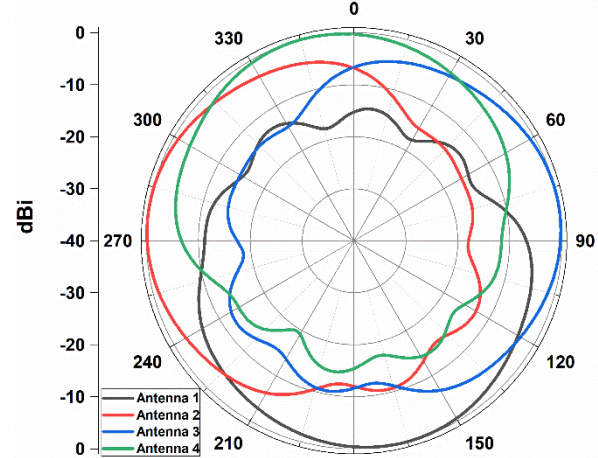


(a) Simulated

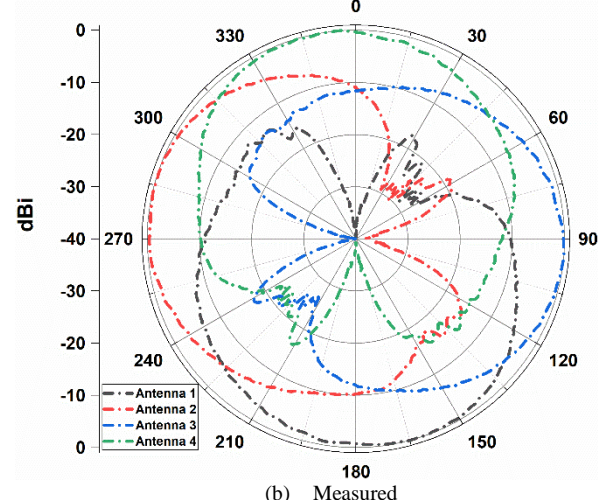


(b) Measured

Fig. 12 Simulated and measured H-plane radiation patterns of the optimized pixelated antennas.



(a) Simulated



(b) Measured

Fig. 13 Simulated and measured E-plane radiation patterns of the optimized pixelated antennas

Fig. 14 represents the simulated and measured H-plane and E-plane radiation pattern of the GPS antenna. The measured realized gain of GPS antenna is 0.9 dBi. Good agreement between the simulated and measured radiation patterns has been observed. The ripples in the measured patterns can be attributed

to the presence of a metal plate in the measurement setup in the anechoic chamber.

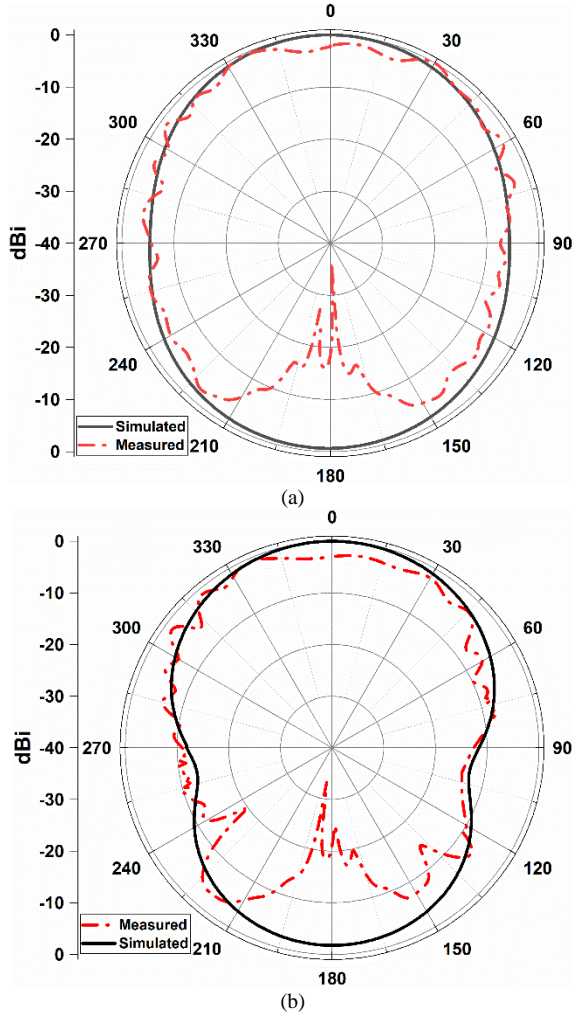


Fig. 14 Radiation patterns of the E-shaped GPS antenna (a) H-plane, (b) E-plane

Fig. 15 illustrates further investigation of the proposed antenna performance on the vehicle roof. Antenna performance can be significantly impacted by the configuration and dimensions of the vehicle roof [25]. A metal plane with 105 cm length and 105 cm width is considered as a vehicle roof. The antenna is then placed on the metal plane. Perfect electric conductor (PEC) is used as the metal plane to reduce the requirement of computational resources. The antenna is placed on the middle of the computational roof model. Simulation is performed considering different gap between the antenna and roof model, denoted by D in Fig. 15. D is varied from 0 to 25 cm. Fig. 16 depicts the impact of the vehicle roof model on the reflection coefficients of the proposed antenna. With varying gaps between the antenna and metal plane, the impedance bandwidth is hardly affected. However, the isolation between antennas has been slightly affected when the antenna is placed closest to the metal plane ($D=0$ cm) as depicted in Fig. 17. The isolation is -30 dB for S21, -27 dB for S31 and -29 dB for S41 at 5.4 GHz, which is still a lot better than the isolation between antennas with standard patch as shown in Fig. 3. However, the maximum isolation is achieved when the gap between antenna and roof is

$D=5$ cm. At this position, S21 is -35 dB, S31 is -41 dB and S41 is -40 dB at 5.4 GHz.

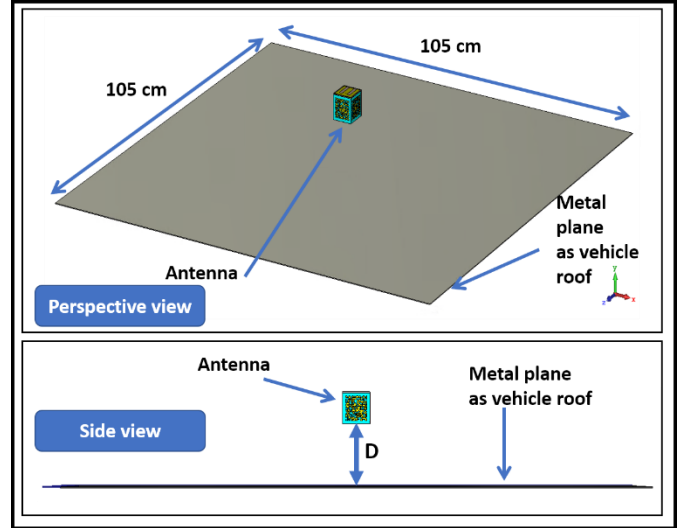


Fig. 15 Simulation of the proposed antenna for vehicular applications considering placement on vehicle roof.

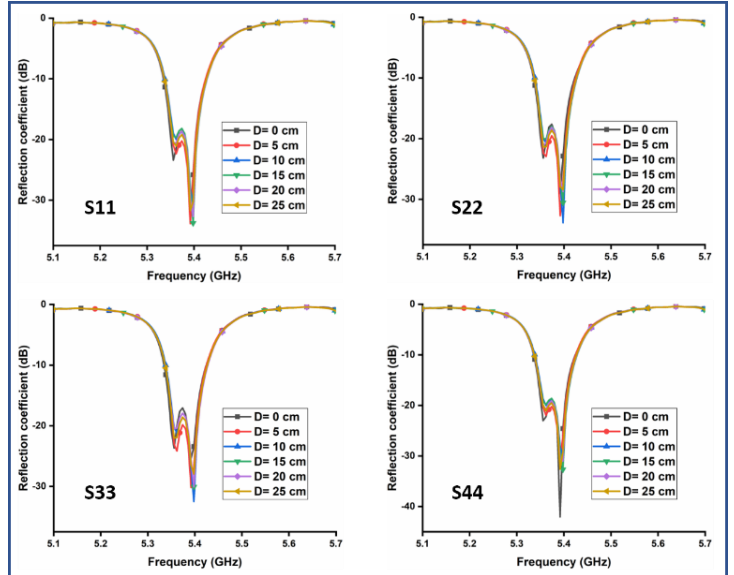


Fig. 16 Reflection coefficients of the antennas (S11, S22, S33, S44)

Radiation patterns of the proposed antenna with metal plane is shown in Fig. 18 when $D=5$ cm. The beamwidths of the patterns are similar to the original radiation patterns in Fig. 12. In summary, although the presence of vehicle roof has negligible impact on the isolation of the proposed antenna, the reflection coefficient and radiation patterns maintain original performance that can contribute to reliable vehicular communications. Also, the minor decrease in isolation when $D=0$ cm is expected as it is the closest position of the antenna to the metal plane. Required isolation level can be maintained by placing the antenna on the vehicle rooftop with a proper gap, such as $D=5$ cm.

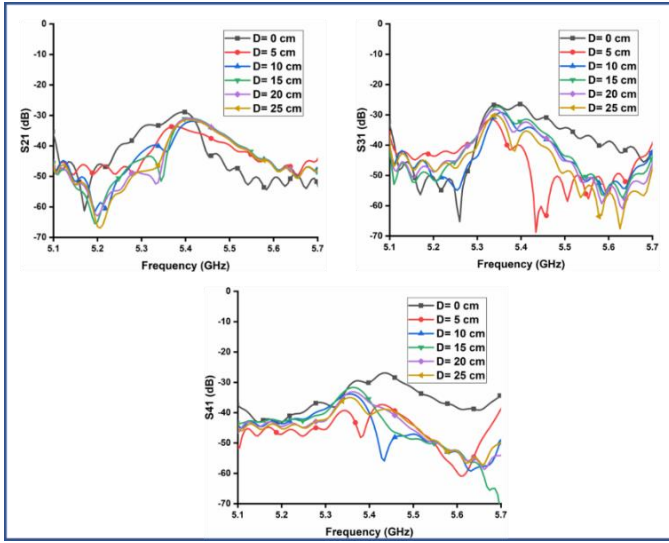


Fig. 17 S-parameters of the antenna with metal plane

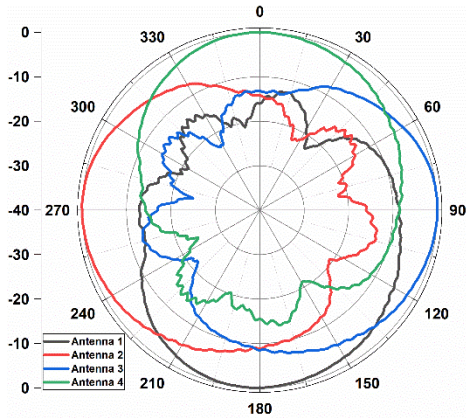


Fig. 18 Radiation patterns of the optimized pixelated antennas with metal plane

Another simulation setup of the proposed antenna is shown in Fig. 19, where the antenna is positioned at the corner of a car roof rack, as it can achieve the highest coverage with least interference from obstacles. Since the roof usually remains open and high above the ground, an automobile's roof or roof rack can be chosen by car manufacturers for the antenna placement. In general, a car's antenna should be placed practically at a higher place off the ground. The position aids in getting a high reception rate in nearly all antenna directions. The simulation setup in Fig. 19 considers a realistic car roof rack. Aluminum has been used as the material of the roof rack. A foam has been considered below the antenna as a holder for the antenna. The height of the foam holder is 2.5 cm. Simulation is performed to investigate the S-parameters and the radiation pattern of the antenna with roof rack. Fig. 20 presents the S-parameters of the antenna when placed at the corner of car roof rack. Reflection coefficients of the antenna is similar to the reflection coefficient of the antenna in free space, resonating at 5.4 GHz for all four antennas. The values of isolation ranges from -32dB to -44 dB for S21, S31 and S41. The isolation is still 18 dB higher in comparison to the results of the antenna with standard patch in free space illustrated previously in Fig.

3. Fig. 21 represents the H plane radiation patterns of the antenna while mounted on the roof rack. There are some apparent ripples in the radiation patterns of antenna 1 and antenna 2, preserving the original radiation patterns in all directions. The slight variations could be attributed to the presence of uneven metallic structure of the vehicle roof rack. Despite the slight alterations brought on by the roof rack arrangement, the antenna radiates effectively within the desired directions as determined by the radiation patterns in free space. The pixelated cubic antenna may be installed in a variety of locations because of its relatively compact structure in relation to the vehicle roof.

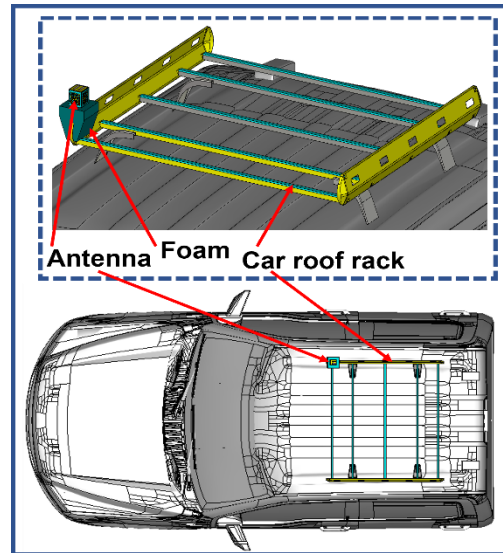


Fig. 19 Simulation of the proposed antenna for vehicular applications considering placement on a car roof rack.

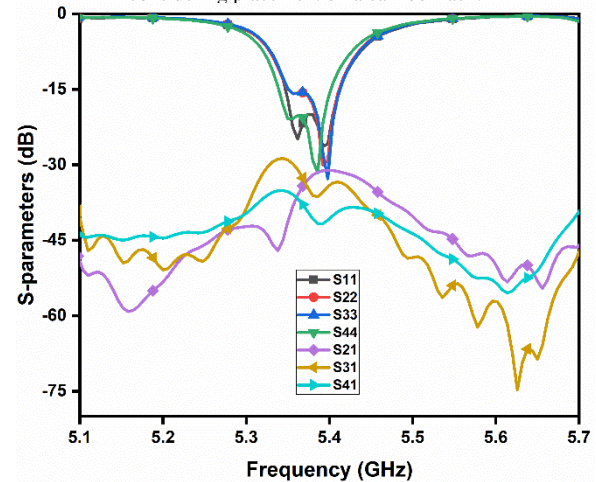


Fig. 20 S-parameters of the proposed antenna when placed on a car roof rack

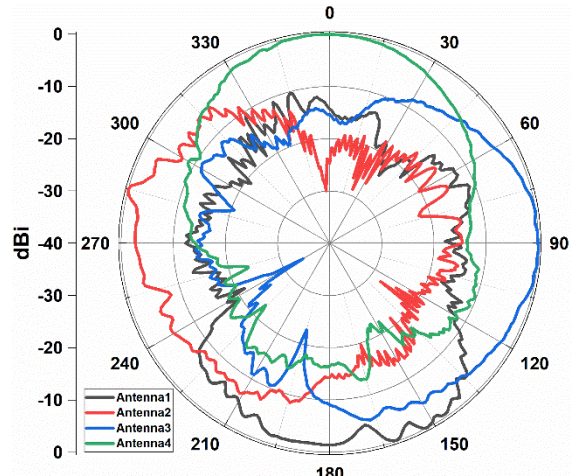


Fig. 21 Radiation patterns of the proposed antenna when placed on a car roof rack

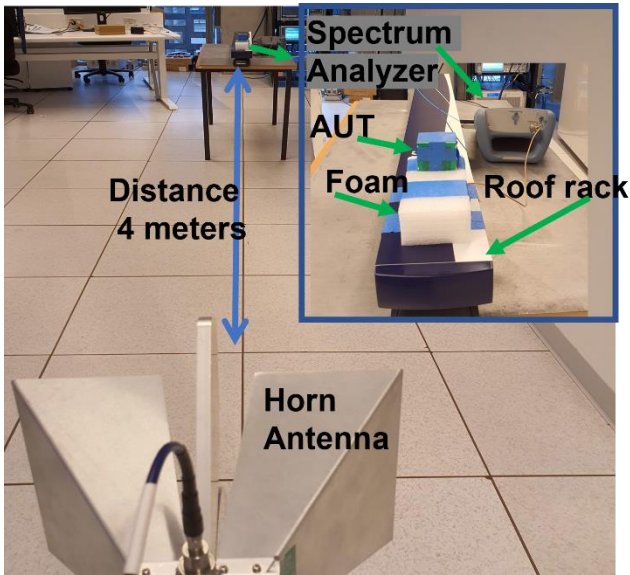
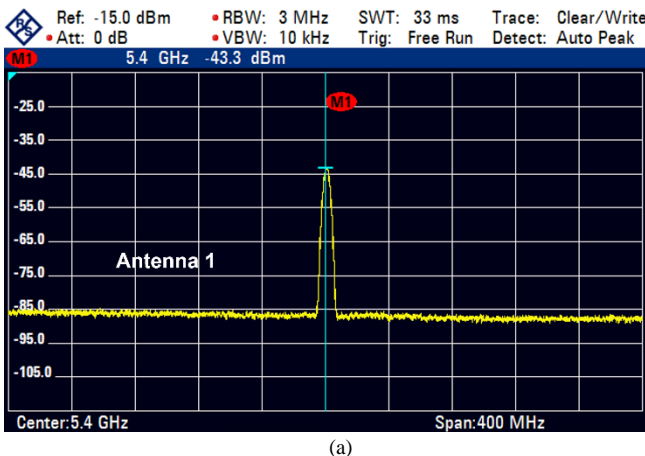
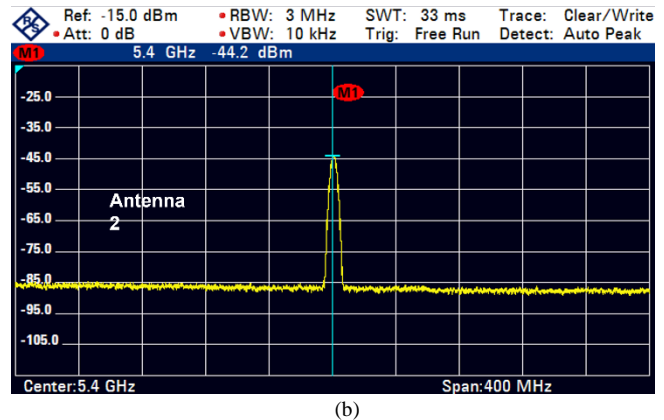


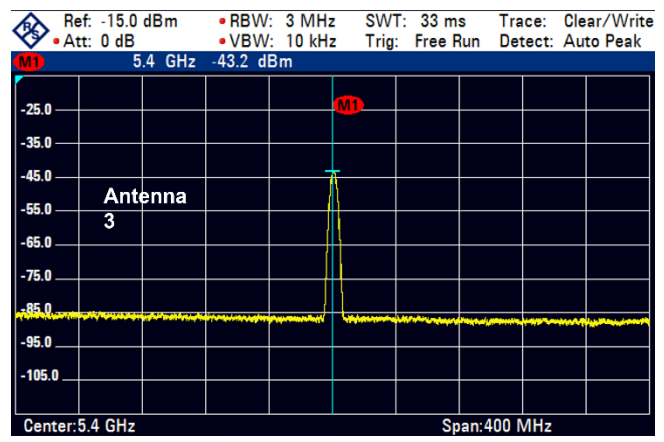
Fig. 22 Experimental setup of power measurement using the proposed antenna as a receiving antenna



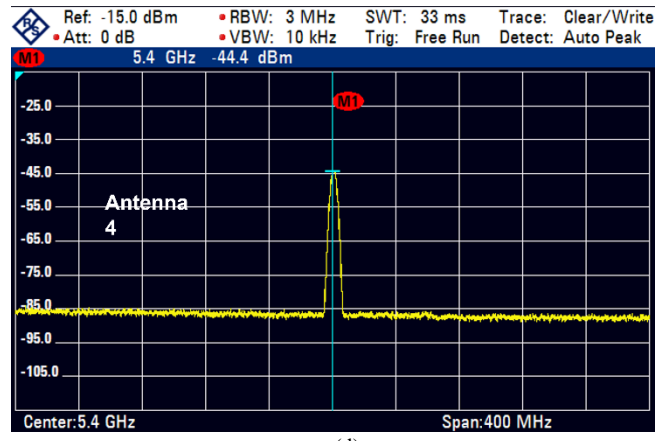
(a)



(b)



(c)



(d)

Fig. 23 Received power by the proposed vehicular antenna; (a) Antenna 1, (b) Antenna 2, (c) Antenna 3, (d) Antenna 4

To demonstrate the potential practical application of the proposed antenna, an experiment has been performed to measure the level of received power of the proposed antenna system with a car roof rack, illustrated in Fig. 22. The antenna has been placed on the car roof rack, while metal plane was placed to represent the metallic car roof right below the roof rack. A signal generator has been used to transfer 0 dBm power at 5.4 GHz using a horn antenna with 10.8 dB gain at 5.4 GHz (Rohde and Schwarz HF907). A spectrum analyzer (Rhode & Schwarz, FSH8, 9 kHz-8 GHz) has been utilized to measure the received signal power level. The received power is measured

for all four antennas by rotating the roof rack to cover all four directions. Four meters distance has been considered between the transmitting horn antenna and the receiving multidirectional pixelated cubic antenna. Fig. 23 depicts the received power level of the four pixelated antennas used in the cubic antenna configuration. The power levels of the Antenna 1, Antenna 2, Antenna 3 and Antenna 4 are -43.3 dBm, -44.2 dBm, -43.2 dBm and -44.4 dBm, respectively. The experimental results prove that the proposed antenna system is capable of receiving wireless signal efficiently, from multiple direction in vehicular or automotive system.

IV. CONCLUSION

In this work, a pixelated multidirectional cubic antenna has been proposed for vehicular applications. The design evolution of the cube shaped antenna is based on a pixelated patch. The design methodology and the results demonstrate the advantages of the cubic configuration and merits of the proposed antenna. The antenna is designed with a binary optimization algorithm to achieve a desired operating band and enhanced isolation. The isolation between antennas has been significantly improved considering the counterpart cubic antenna design with standard patch configuration. High isolation is achieved without using any additional hardware or filters, while the measured gain in each direction is about 6.4 dBi. The antenna performance has also been investigated by placing the antenna on a vehicle roof and roof rack model in EM simulator and in measurement. The antenna performance is nearly unaffected by the presence of a metal plane on the vehicle roof and roof rack. There is no requirement for metallic components or grounding on the bottom side of the antenna which simplifies installation at different areas of the vehicle. Featuring compact size, enhanced isolation, multidirectional radiation pattern, lightweight, low cost, straightforward design, and simple manufacturing, the proposed antenna is well-suited for vehicle systems.

REFERENCES

- [1] R. Keshavarz, A. Mohammadi and A. Abdipour, "Linearity improvement of a dual-band Doherty power amplifier using E-CRLH transmission line, *AEU - International Journal of Electronics and Communications*, Vol. 131, 2021.
- [2] L. Liang, H. Peng, G. Y. Li, and X. Shen, "Vehicular communications: A physical layer perspective," *IEEE Transactions on Vehicular Technology*, vol. 66, no. 12, pp. 10647-10659, 2017.
- [3] R. Keshavarz, D. Winson, J. Lipman, M. Abolhasan, and N. Shariati, "Dual-Band, Slant-Polarized MIMO Antenna Set for Vehicular Communication," in *2023 17th European Conference on Antennas and Propagation (EuCAP)*, 2023: IEEE, pp. 1-5.
- [4] M. Bilgic and K. Yegin, "Modified annular ring antenna for GPS and SDARS automotive applications," *IEEE Antennas and Wireless Propagation Letters*, vol. 15, pp. 1442-1445, 2015.
- [5] Q. Wu, Y. Zhou, and S. Guo, "An L-sleeve L-monopole antenna fitting a shark-fin module for vehicular LTE, WLAN, and car-to-car communications," *IEEE Transactions on Vehicular Technology*, vol. 67, no. 8, pp. 7170-7180, 2018.
- [6] J.-K. Che, C.-C. Chen, and J. F. Locke, "A compact four-channel MIMO 5G sub-6 GHz/LTE/WLAN/V2X antenna design for modern vehicles," *IEEE Transactions on Antennas and Propagation*, vol. 69, no. 11, pp. 7290-7297, 2021.
- [7] M. A. Ullah, R. Keshavarz, M. Abolhasan, J. Lipman, K. P. Esselle, and N. Shariati, "A Review on Antenna Technologies for Ambient RF Energy Harvesting and Wireless Power Transfer: Designs, Challenges and Applications," *IEEE Access*, 2022.
- [8] B. R. Jackson, S. Rajan, B. J. Liao, and S. Wang, "Direction of arrival estimation using directive antennas in uniform circular arrays," *IEEE Transactions on Antennas and propagation*, vol. 63, no. 2, pp. 736-747, 2014.
- [9] C.-H. Ou, B.-Y. Wu, and L. Cai, "GPS-free vehicular localization system using roadside units with directional antennas," *Journal of Communications and Networks*, vol. 21, no. 1, pp. 12-24, 2019.
- [10] T. Mondal, S. Maity, R. Ghatak, and S. R. B. Chaudhuri, "Compact circularly polarized wide-beamwidth fern-fractal-shaped microstrip antenna for vehicular communication," *IEEE Transactions on Vehicular Technology*, vol. 67, no. 6, pp. 5126-5134, 2018.
- [11] C.-Y. Chiu, C.-H. Cheng, R. D. Murch, and C. R. Rowell, "Reduction of mutual coupling between closely-packed antenna elements," *IEEE transactions on antennas and propagation*, vol. 55, no. 6, pp. 1732-1738, 2007.
- [12] M. G. N. Alsath *et al.*, "An integrated tri-band/UWB polarization diversity antenna for vehicular networks," *IEEE Transactions on Vehicular Technology*, vol. 67, no. 7, pp. 5613-5620, 2018.
- [13] S. Xiao, M.-C. Tang, Y.-Y. Bai, S. Gao, and B.-Z. Wang, "Mutual coupling suppression in microstrip array using defected ground structure," *IET microwaves, antennas & propagation*, vol. 5, no. 12, pp. 1488-1494, 2011.
- [14] Y. Liu, X. Yang, Y. Jia, and Y. J. Guo, "A low correlation and mutual coupling MIMO antenna," *IEEE Access*, vol. 7, pp. 127384-127392, 2019.
- [15] M. Ullah, R. Keshavarz, M. Abolhasan, J. Lipman, and N. Shariati, "Low-profile dual-band pixelated defected ground antenna for multistandard IoT devices," *Scientific Reports*, vol. 12, no. 1, pp. 1-19, 2022.
- [16] A. Habashi, J. Nourinia, and C. Ghobadi, "Mutual coupling reduction between very closely spaced patch antennas using low-profile folded split-ring resonators (FSRRs)," *IEEE antennas and wireless propagation letters*, vol. 10, pp. 862-865, 2011.
- [17] J. Mu'Ath, T. A. Denidni, and A. R. Sebak, "Millimeter-wave compact EBG structure for mutual coupling reduction applications," *IEEE Transactions on Antennas and Propagation*, vol. 63, no. 2, pp. 823-828, 2014.
- [18] B. L. Dhevi, K. S. Vishvaksenan, and K. Rajakani, "Isolation enhancement in dual-band microstrip antenna array using asymmetric loop resonator," *IEEE Antennas and Wireless Propagation Letters*, vol. 17, no. 2, pp. 238-241, 2017.
- [19] M. G. N. Alsath, M. Kanagasabai, and B. Balasubramanian, "Implementation of slotted meander-line resonators for isolation enhancement in microstrip patch antenna arrays," *IEEE Antennas and Wireless Propagation Letters*, vol. 12, pp. 15-18, 2012.
- [20] R. Keshavarz, M. Movahhedi, A. Hakimi and A. Abdipour, "A Novel Broad Bandwidth and Compact Backward Coupler with High Couplinglevel," *Journal of Electromagnetic Waves and Applications*, vol. 25, no. 2, pp. 283-293, 2018.
- [21] A. Ghadimi, V. Nayyeri, M. Khanjarian, M. Soleimani, and O. M. Ramahi, "A systematic approach for mutual coupling reduction between microstrip antennas using pixelization and binary optimization," *IEEE Antennas and Wireless Propagation Letters*, vol. 19, no. 12, pp. 2048-2052, 2020.
- [22] R. Keshavarz, Y. Miyanaga, M. Yamamoto, T. Hikage and N. Shariati, "Metamaterial-Inspired Quad-Band Notch Filter for LTE Band Receivers and WPT Applications," 2020 XXXIIrd General Assembly and Scientific Symposium of the International Union of Radio Science, Rome, Italy, 2020, pp. 1-4, doi: 10.23919/URSIGASS49373.2020.9232331.
- [23] M. A. Ullah, R. Keshavarz, M. Abolhasan, J. Lipman and N. Shariati, "Multiservice Compact Pixelated Stacked Antenna With Different Pixel Shapes for IoT Applications," in *IEEE Internet of Things Journal*, vol. 10, no. 22, pp. 19883-19897, 15 Nov. 2023.
- [24] S. Mirjalili and A. Lewis, "S-shaped versus V-shaped transfer functions for binary particle swarm optimization," *Swarm and Evolutionary Computation*, vol. 9, pp. 1-14, 2013.
- [25] A. Kwoczek, Z. Raida, J. Láćik, M. Pokorný, J. Puskely, and P. Vágner, "Influence of car panorama glass roofs on Car2Car communication (poster)," in *2011 IEEE Vehicular Networking Conference (VNC)*, 2011: IEEE, pp. 246-251.



Md. Amanath Ullah (S'19) is a PhD candidate at the School of Electrical and Data Engineering, University of Technology Sydney (UTS). He completed M.Sc. by research in Electrical, Electronic and System Engineering from The National University of Malaysia in 2019. He worked as a Graduate Research Assistant at the Microwave Laboratory, The National University of Malaysia from 2016 to 2019. His current research interest includes, antenna design and technology, antenna optimization, wireless power transmission (WPT), radio frequency energy harvesting (RFEH) and self-powered sensors/devices.



Rasool Keshavarz (M) was born in Shiraz, Iran, in 1986. He received the Ph.D. degree in Telecommunications Engineering from the Amirkabir University of Technology, Tehran, Iran, in 2017. He is currently working as a Postdoctoral Research Fellow with the RFCT Laboratory, University of Technology Sydney, Australia. His main research interests include RF and microwave circuit and system design, sensors, antenna design, wireless power transfer (WPT), and RF energy harvesting (EH).



Justin Lipman (S'94, M'04, SM'12) received a PhD in Telecommunications Engineering from University of Wollongong, Australia in 2004. He is an Industry Associate Professor at the University of Technology Sydney (UTS) and a visiting Associate Professor at Hokkaido University's Graduate School of Engineering. He is the Director of Research Translation in the Faculty of Engineering and IT and is Director of the RF Communications Technologies (RFCT) Lab - where he leads industry engagement in RF technologies, Internet of Things, Tactile Internet and Software Defined Communication. He serves as committee member in Standards Australia contributing to International IoT standards and Digital Twins. Prior to joining UTS, he was based in Shanghai, China and held a number of senior management and technical leadership roles at Intel and Alcatel driving research and innovation, product development, architecture and IP generation. He is an IEEE Senior Member. His research interests are in all “things” adaptive, connected, distributed and ubiquitous.



Mehran Abolhasan (M'03-SM'11) is an Associate Professor in the University of Technology, Sydney. He has expertise in a number of different areas including: IoT and Sensor Network Technologies, Wireless Networking and Analytics, Software Defined Networking, Algorithm Development, Simulation and Modelling and development of Test-beds. His experience and contribution to the above areas has resulted in significant research outcomes, which have been published in highly prestigious IEEE journals and achieving high citations. He has authored over 170 international publications and has won over six million dollars in research funding. He has led and worked as a Chief Investigator on a diverse range of projects including: ARC Discovery Project, ARC Linkage, ARC LIEF, CRC and various government and Industry funded projects. He has served in various leadership roles over the past 10 years, including: serving as a Director of Research programs in the Faculty of Engineering and IT, representing Australia as the head of Delegates for ISO/IEC IoT Standardisation meetings and serving as the Deputy Head of School for Research in the School of Electrical and Data Engineering. He is currently a Senior Member of IEEE and regularly serves as a reviewer for various IEEE, ACM and Elsevier journals. He also serves many conferences as a reviewer, TPC and Organiser. His current research Interests are in Software Defined Networking, IoT, WSNs, Intelligent Transportation Systems, Wireless Multi-hop Networks, 5G/6G Networks and Beyond.



Negin Shariati (M) is a Senior Lecturer in the School of Electrical and Data Engineering, Faculty of Engineering and IT, University of Technology Sydney (UTS), Australia. She established the state of the art RF and Communication Technologies (RFCT) research laboratory at UTS in 2018, where she is currently the Co-Director and leads research and development in RF Technologies, Sustainable Sensing, Energy Harvesting, Low-power Internet of Things and AgTech. She leads the Sensing Innovations Constellation at Food Agility CRC (Corporative Research Centre), enabling new innovations in agriculture technologies by focusing on three key interrelated streams; Sensing, Energy and Connectivity. Since 2018, she has held a joint appointment as a Senior Lecturer at Hokkaido University, externally engaging with research and teaching activities in Japan. Negin Shariati was the recipient of Standout Research Award in the 2021 IoT Awards Australia, and IEEE Victorian Section Best Research Paper Award 2015. She attracted over two million dollars worth of research funding across a number of CRC and industry projects, where she has taken the lead CI (Chief Investigator) role and also contributed as a member of the CI team. Dr Shariati completed her PhD in Electrical-Electronics and Communication Technologies at Royal Melbourne Institute of Technology (RMIT), Australia, in 2016. She worked in industry as an Electrical-Electronics Engineer from 2009-2012. Her research interests are in RF-Electronics Circuits and Systems, Sensors, Antennas, RF Energy Harvesting, Simultaneous Wireless Information and Power Transfer, and Wireless Sensor Networks.